J. Fluid Mech. (1971), *vol.* 50, *part* 1, *pp.* 107–132
Printed in Great Britain

Weak quadratic interactions of two-dimensional waves

By YOUNG YUEL KIM AND THOMAS J. HANRATTY
Department of Chemical Engineering, University of Illinois, Urbana, Illinois

(Received 9 April 1970 and in revised form 24 February 1971)

This paper reports on weak quadratic interactions which can occur with two-dimensional waves on shallow water layers and in the capillary–gravity range on deep water layers. It supplies experimental support of theoretical predictions for resonant interactions, but, perhaps of more significance, it explores in detail interactions which occur under conditions near resonance.

Waves of approximately sinusoidal form are introduced on the surface of water in a long rectangular tank. For deep water a rapid distortion in the sinusoidal wave and sometimes additional crests are observed because of energy exchange among the first, second and third harmonics at frequencies where both surface tension and gravity are important (7·5–13 c/s). An even greater exchange of energy can be observed on shallow water layers at low frequencies. For example, a wave train with seven secondary crests can be observed when the wave maker is operated at 3·04 c/s in a water layer of 0·65 cm.

Measured amplitudes and phase angles of the Fourier components of the wave train are described by a system of equations using only quadratic interactions among participating harmonics. The exchange of energy among Fourier components under certain conditions is explained in terms of the rate of change of relative phase angles of the different harmonics.

1. Introduction

The surface profile of waves propagating at a gas–liquid interface may be viewed as consisting of a number of Fourier components. One of the salient features of finite amplitude waves is that these Fourier components can exchange energy. In 1960, Phillips introduced the notion that energy exchange can be greatly facilitated by a resonant interaction. He considered gravity waves and showed that such interactions can occur at third order on deep water and at second order on shallow water. McGoldrick (1965) later found second-order resonance for capillary–gravity waves on deep water.

Resonance theory has been exploited in a number of laboratory investigations. Benjamin & Feir (1967) carried out experiments which show that finite amplitude progressive gravity waves are unstable because of third-order resonant interactions between the primary Fourier harmonic and side-band frequencies. McGoldrick, Phillips, Huang & Hodgson (1966) and Longuet-Higgins & Smith (1966) have measured the initial growth of a free gravity wave formed on deep water by the resonant interaction of two primary free oscillations. McGoldrick (1970) succeeded recently in demonstrating the resonant interaction of two-

dimensional capillary–gravity waves on deep water at $n = g/k^2T = 2$ (9·85 c/s for water at 25 °C), where k is the wave-number, g the acceleration of gravity, and T the quotient of the surface tension and the density.

This paper reports on weak quadratic interactions which can occur with waves on shallow liquid layers and with waves in the capillary–gravity range on deep liquid layers. It demonstrates that significant interactions are not confined just to resonance conditions, but are realizable over a range of frequencies in the neighbourhood of resonance. Results on resonant interactions, presented in this paper as a special case, extend the recent study of McGoldrick (1970) in that the effect of depth on resonance is examined and phase angles as well as amplitudes of interacting components are measured. Some of the difficulties experienced by McGoldrick with respect to surface contamination were avoided; because of this the second harmonic was not dampened as rapidly and a more direct comparison between theory and experiment is possible.

We present results on both stationary and transient wave phenomena. In the experiments on stationary phenomena waves were generated by an oscillating dipper in the centre of a long rectangular tank containing water and the surface profile was studied at different distances from the dipper by measuring the amplitudes and phase angles of the Fourier harmonics. The dipper motion was carefully controlled so that the wave profile near the dipper was very close to a sinusoidal shape and absorbing beaches were located at both ends of the tank. In the transient experiments an amplitude modulated sinusoidal wave packet was introduced on the water by a high potential electric field.

If the dipper is operated at 5 c/s in a deep water layer the wave profile at different distances from the wave maker does not change its form dramatically. If the frequency of the dipper is increased so that surface tension becomes more important, higher-order harmonics appear near the wave maker and these can be large enough that additional crests are observed. These effects are particularly evident close to the second-order resonance condition, $n = 2$, where there is a monotonic transfer from the first to the second harmonic; but, in general, they are observed over a frequency range which depends on the initial wave steepness. Waves of permanent form of the type predicted by Wilton (1915) and by Pierson & Fife (1961) were not realized since the specific initial conditions required for waves of permanent form were not met. All waves with additional crests were found to change their shapes continuously as they propagated downstream. In the transient experiments dramatic changes in the wave packet occurred close to $n = 2$. Initially the sinusoidal waves were distorted by the growth of the second harmonic; this harmonic propagated faster than the primary and concentrated in the front part of the packet.

The resonant frequency at which a large monotonic transfer of energy from the first to the second harmonic occurred could be decreased by using a shallow liquid layer. However, if the layer was too shallow, growth of higher harmonics obscured this clear-cut transfer from the first to the second harmonic. The large exchange of energy in shallow layers can be demonstrated either by decreasing the frequency of the dipper, keeping the water layer at a constant height of about 0·75 cm, or by decreasing the height of the water layer while the frequency

of the dipper is at 5 c/s. Consider the latter case. At a height of about 1 cm very little distortion of the sinusoidal wave is observed. At heights between about 0·7 and 0·85 cm a large growth of second harmonic occurs near the wave maker. At greater distances from the wave maker progressively higher harmonics appear in the wave pattern. For example, at a height of 0·79 cm waves with five crests are observed over the period of the wave maker at a distance of 26 cm from the wave maker. As the layer height is decreased further the number of harmonics that are present in the pattern in significant amounts decreases.

The surface displacement η may be described by the equation

$$\eta = \sum_{\alpha=0}^{N} a_\alpha \cos(\alpha\theta + \gamma_\alpha), \tag{1}$$

where a_α is the amplitude of the αth harmonic, $\theta = kx - \omega t$, k is the wave-number, ω the frequency, x the co-ordinate in the direction of propagation, t the time and γ_α the phase angle. The experiments are interpreted by a system of quadratic interaction equations derived by assuming that a_α and γ_α in (1) are functions of time. The calculated variations with respect to time are related to the distance from the wave maker by use of a group velocity. The effects of viscosity are assumed to be independent of the non-linear interactions. Equations for the variation of a_α and γ_α with time are obtained by making use of the assumption of irrotational flow and the non-linear boundary conditions at the interface, as proposed by Simmons (1969). The chief differences are that *a priori* assumptions about the magnitude of the a_α's are not made and that the resulting equations can be applied over a range of frequencies, including the resonance case.

In the context of this formulation the large exchange of energy among Fourier components observed under certain conditions is explained in terms of the rate of change of the relative phases of the different harmonics.

2. Inviscid analysis

In developing the interaction equations we found it more convenient to represent the displacement $\eta(x,t)$ and the velocity potential $\Phi(x,y,t)$ by Fourier series with complex coefficients. Hence

$$\eta = \sum_{\alpha=0}^{N} A_\alpha e^{i\alpha\theta} + A_\alpha^* e^{-i\alpha\theta}, \tag{2}$$

$$\Phi = \sum_{\alpha=1}^{N} B_\alpha \frac{\cosh \alpha k(y+h)}{\sinh \alpha kh} e^{i\alpha\theta} + \text{complex conjugate}, \tag{3}$$

where h is the depth of the water, A_α and B_α are functions of time and * designates the complex conjugate. The amplitudes and phase angles of various harmonics are then expressed as

$$a_\alpha^2 = 4A_\alpha^* A_\alpha, \tag{4}$$

$$\gamma_\alpha = \cos^{-1}(2A_{\alpha R}/a_\alpha), \tag{5}$$

where $A_{\alpha R} = \frac{1}{2}(A_\alpha + A_\alpha^*)$. A system of differential equations for the coefficients A_α may be obtained by substitution of (2) and (3) into the non-linear boundary conditions

$$-T\frac{\partial^2\eta}{\partial x^2} + g\eta - \frac{\partial\Phi}{\partial t} - \frac{\partial^2\Phi}{\partial t\,\partial y}\eta + \frac{1}{2}\left\{\left(\frac{\partial\Phi}{\partial x}\right)^2 + \left(\frac{\partial\Phi}{\partial y}\right)^2\right\} = 0, \tag{6}$$

$$\frac{\partial \eta}{\partial t}-\frac{\partial \Phi}{\partial x}\frac{\partial \eta}{\partial x}+\frac{\partial \Phi}{\partial y}+\frac{\partial^2 \Phi}{\partial y^2}\eta = 0, \tag{7}$$

to be satisfied at $y = 0$. Triple product terms are neglected in (6) and (7) since the experimental results are to be interpreted only in terms of quadratic interactions. From (2), (3) and (7) the B_α's can be expressed in terms of the A_α's and their derivatives. Using this result and (6) the following differential equations have been derived for the variation of A_α with ξ, where $\xi = \omega t$.

$$\left.\begin{aligned} A_{1,\xi} &= 4ik(P_1 A_1^* A_2 + P_2 A_2^* A_3 + P_3 A_3^* A_4) = \text{right-hand side of (1)},\\ A_{2,\xi} &= iL_2 A_2 - 2ik(P_4 A_1^2 + P_5 A_1^* A_3 + P_6 A_2^* A_4) = \text{right-hand side of (2)},\\ A_{3,\xi} &= iL_3 A_3 - \tfrac{4}{3}ik(P_7 A_2 A_1 + P_8 A_1^* A_4) = \text{right-hand side of (3)},\\ A_{4,\xi} &= iL_4 A_4 - ik(P_9 A_1 A_3 + P_{10} A_2^2) = \text{right-hand side of (4)}, \end{aligned}\right\} \tag{8}$$

where

$$\omega^2 = (gk + k^3 T)\tanh(kh), \tag{9}$$

$$L_\alpha = \frac{\alpha}{2} - \frac{gk + \alpha^2 k^3 T}{2[\alpha K]\,\omega^2} \tag{10}$$

and

$$\left.\begin{aligned} P_1 &= (1/8[K])([K]^2 + 4[K][2K] - 3),\\ P_2 &= (1/8[K])(2[K][2K] + 3[K][3K] + 6]2K][3K] - 7),\\ P_3 &= (1/8[K])(4[K][4K] + 3[K][3K] + 12[3K][4K] - 13),\\ P_4 &= ([K]/[2K])P_1,\\ P_5 &= (1/8[2K])(4[K][2K] + 12[2K][3K] + 6[K][3K] - 14),\\ P_6 &= (1/8[2K])(8[2K]^2 + 32[2K][4K] - 24),\\ P_7 &= (1/8[3K])(9[K][3K] + 6[K][2K] + 18[2K][3K] - 21),\\ P_8 &= (1/8[3K])(9[K][3K] + 12[K][4K] + 36[3K][4K] - 39),\\ P_9 &= (1/8[4K])(16[K][4K] + 48[3K][4K] + 12[K]3[K] - 52),\\ P_{10} &= (1/8[4K])(32[2K][4K] + 8[2K]^2 - 24). \end{aligned}\right\} \tag{11}$$

Here $[\alpha K] = \coth \alpha kh$.

It is to be noted that second derivatives $A_{\alpha,\xi\xi}$ and non-linear terms like $A_{\alpha,\xi}A_\beta^*$ are neglected compared to $A_{\alpha,\xi}$. This simplification can be justified by using a two-time scale expansion discussed by Benney (1962) and Bretherton (1964). A more direct confirmation of the accuracy of this assumption can be obtained by comparing, for a number of cases, numerical integrations of the complete equations with numerical integrations of the simplified equations (Kim 1970). Results for $n = 2$ for an initially sinusoidal wave with $ka_1 = 0{\cdot}1$ are shown in figure 1.

Because of the complexity of the algebra, we have considered only the first four harmonics. Therefore equations (8) will not describe situations where fifth or higher harmonics become significant. These equations can be accurate only to second order, $O(\epsilon^2)$, where $\epsilon = ka_\alpha$ and a_α is the Fourier component with the largest amplitude. Some of the quadratic products are of much higher order than second, and further simplification of (8) is possible if we apply assumptions about the order of magnitude of some of the Fourier components, but this method

of ordering will depend on the frequency and on the height of the liquid layer so the simplified form of (8) will depend on the conditions being considered. Since we are interested in interpreting experiments which cover a wide range of variables and since we shall be considering cases in which higher harmonics grow to the same magnitude as the first, we have not found it convenient to attempt any further simplification of (8).

The first approximation of the total wave energy associated with the αth harmonic averaged over one wavelength is

$$E_\alpha = \alpha I_\alpha a_\alpha^2, \tag{12}$$

where

$$I_\alpha = \frac{\pi\rho}{2k^2}\left(\omega^2[\alpha K] + \frac{gk}{\alpha} + \alpha k^3 T\right) \tag{13}$$

and ρ is the fluid density. The following relations are obtained from equations (8) and their complex conjugates:

$$\left.\begin{aligned}
dE_1/d\xi &= I_1\{P_1 a_1^2 a_2 \sin(\gamma_2 - 2\gamma_1) + P_2 a_1 a_2 a_3 \sin(\gamma_3 - \gamma_1 - \gamma_2) \\
&\quad + P_3 a_1 a_3 a_4 \sin(\gamma_4 - \gamma_1 - \gamma_3)\}, \\
dE_2/d\xi &= I_2^3 P_4 a_1^2 a_4 \sin(2\gamma_1 - \gamma_2) + P_5 a_1 a_2 a_3 \sin(\gamma_3 - \gamma_1 - \gamma_2) \\
&\quad + P_6 a_2^2 a_4 \sin(\gamma_4 - 2\gamma_2)\}, \\
dE_3/d\xi &= I_3\{P_7 a_1 a_2 a_3 \sin(\gamma_1 + \gamma_2 - \gamma_3) + P_8 a_1 a_3 a_4 \sin(\gamma_4 - \gamma_1 - \gamma_3)\}, \\
dE_4/d\xi &= I_4\{P_9 a_1 a_3 a_4 \sin(\gamma_1 + \gamma_3 - \gamma_4) + P_{10} a_2^2 a_4 \sin(2\gamma_2 - \gamma_4)\}.
\end{aligned}\right\} \tag{14}$$

From (14) we can see that the rate and the direction of energy exchange depend on the relative phase angles of different Fourier harmonics. For example, when only the primary and the secondary harmonics are considered, the maximum rate of energy exchange between the first and the second harmonic occurs when the relative phase angle $(\gamma_2 - 2\gamma_1)$ is equal to $\pm\frac{1}{2}\pi$. To have a large net transfer of energy between Fourier harmonics it is necessary not only to have a favourable phase-angle relation but also a slow rate of change of the relative phase angles. If the time constant governing the cyclic change of the relative phase of the different harmonics is small compared to $1/\omega$, then any transfer of energy from one component to the other during part of the cycle is counterbalanced by transfer in the opposite direction during the other part of the cycle. If this time constant is large compared to $1/\omega$, then there can be a relatively large net exchange of energy. The rate of change of the phase angles can be derived from (5) and (8). From (5) we have

$$\frac{d\gamma_\alpha}{d\xi} = \frac{4(A_{\alpha i} A_{\alpha R,\xi} - A_{\alpha R} A_{\alpha i,\xi})}{a_\alpha^2}, \tag{15}$$

where $A_{\alpha i} = \frac{1}{2}i(A_\alpha^* - A_\alpha)$. We assume that the A_α's are not zero and eliminate $A_{\alpha i,\xi}$ and $A_{\alpha R,\xi}$ by using (8) to obtain

$$\frac{d\gamma_1}{d\xi} = -2k\left\{P_1 a_2 \cos(\gamma_2 - 2\gamma_1) + P_2 \frac{a_2 a_3}{a_1}\cos(\gamma_3 - \gamma_1 - \gamma_2) + P_3 \frac{a_3 a_4}{a_1}\cos(\gamma_4 - \gamma_3 - \gamma_1)\right\}, \tag{16}$$

which may be interpreted as a correction to the linear dispersion relation (Simmons 1969), and

$$\left.\begin{aligned}
\frac{d\gamma_2}{d\xi} &= L_2 - k\left\{P_4\frac{a_1^2}{a_2}\cos(\gamma_2-2\gamma_1)+\frac{P_5 a_1 a_3}{a_2}\cos(\gamma_3-\gamma_1-\gamma_2)+P_6 a_4\cos(\gamma_4-2\gamma_2)\right\},\\
\frac{d\gamma_3}{d\xi} &= L_3 - \tfrac{2}{3}k\left\{\frac{P_7 a_1 a_2}{a_3}\cos(\gamma_3-\gamma_1-\gamma_2)+\frac{P_8 a_1 a_4}{a_3}\cos(\gamma_4-\gamma_1-\gamma_3)\right\},\\
\frac{d\gamma_4}{d\xi} &= L_4 - \frac{k}{2}\left\{\frac{P_9 a_1 a_3}{a_4}\cos(\gamma_4-\gamma_1-\gamma_3)+\frac{P_{10}a_2^2}{a_4}\cos(\gamma_4-2\gamma_2)\right\}.
\end{aligned}\right\} \tag{17}$$

The first terms on the right side of (17) are independent of the amplitudes and will be designated the linear terms. When L_α vanishes, the αth harmonic is a free oscillation; i.e. αk and $\alpha\omega$ satisfy the linear dispersion relation (9). The rate of change of the relative phase angles appearing in (14) can now be calculated from (16) and (17). For example, the rates of change of $(\gamma_2-2\gamma_1)$ and $(\gamma_3-\gamma_2-\gamma_1)$ are

$$\left.\begin{aligned}
\frac{d}{d\xi}(\gamma_2-2\gamma_1) &= L_2 + k\left\{\left(4P_1 a_2-\frac{P_4 a_1^2}{a_2}\right)\cos(\gamma_2-2\gamma_1)\right.\\
&\qquad +\left(\frac{4P_2 a_2 a_3}{a_1}-\frac{P_5 a_1 a_3}{a_2}\right)\cos(\gamma_3-\gamma_1-\gamma_2)\Big\}\\
&\qquad +\frac{4P_3 a_3 a_4}{a_1}a_4\cos(\gamma_4-\gamma_3-\gamma_1)-P_6 a_4\cos(\gamma_4-2\gamma_2)\Big\},\\
\frac{d}{d\xi}(\gamma_3-\gamma_2-\gamma_1) &= (L_3-L_2)+k\left\{\left(\frac{P_4 a_1^2}{a_2}+2P_1 a_2\right)\cos(\gamma_2-2\gamma_1)\right.\\
&\qquad +\left(\frac{2P_2 a_2 a_3}{a_1}+\frac{P_5 a_1 a_3}{a_2}-\frac{2P_7 a_1 a_2}{3a_3}\right)\cos(\gamma_3-\gamma_2-\gamma_1)\\
&\qquad +\left(\frac{2P_3 a_3 a_4}{a_1}+\frac{2P_8 a_1 a_4}{3a_3}\right)\cos(\gamma_4-\gamma_1-\gamma_3)+P_6 a_4\cos(\gamma_4-2\gamma_2)\Big\}.
\end{aligned}\right\} \tag{18}$$

It is seen from (18) that the relative phase angles can change both because of linear terms, ΔL_α, and non-linear terms which depend on the amplitudes of the participating Fourier components. Since the experiments are carried out under conditions such that the initial $a_1 k$ is a small number, the non-linear terms are small over most of the cycle of energy exchange. They are large only during time intervals when the amplitude of one of the harmonics is close to zero. The changes that occur here correspond to the staircase-like phase angle relation with jumps of π at the zeros of a_2 discussed by Simmons (1969) for his case of $C \to 0$. Consider the first of (18) at $\xi = 0$ when the wave on the surface is sinusoidal:

$$\frac{d}{d\xi}(\gamma_2-2\gamma_1) = -P_4\frac{a_1^2}{a_2}\cos(\gamma_2-2\gamma_1)+L_2, \tag{19}$$

where $P_4(a_1^2/a_2)$ is a very large number. For $L_2 = 0$, (19) is the same equation considered by Simmons (1969). In order to illustrate the behaviour of (19) we

will use the following equation which is a reasonable model provided M is a large number but not infinite:

$$d(\gamma_2-\gamma_1)/d\xi = M\cos(\gamma_2-2\gamma_1). \tag{20}$$

The solution to (20) is

$$\tan\{\tfrac{1}{2}(\gamma_2-2\gamma_1)+\tfrac{1}{4}\pi\} = C_0\exp\{-P_4(a_1^2/a_2)\,\xi\}. \tag{21}$$

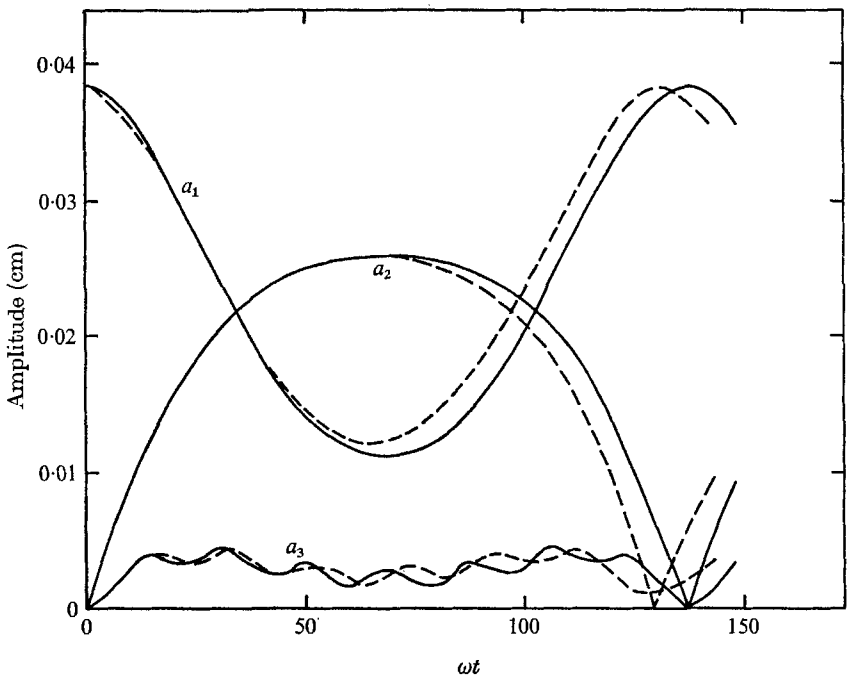

FIGURE 1. Calculated variations of amplitudes for $n = 2$, $ka_1 = 0{\cdot}1$. ——, simplified using 2 time scales; – –, complete equations.

When $a_2 \to 0$ the relative phase angle $(\gamma_2-2\gamma_1)$ is predicted to approach $-\frac{1}{2}\pi$ at an exponential rate where a maximum rate of growth of the second harmonic is predicted by (14). If $L_2 = 0$ and only the first two harmonics are considered, $(\gamma_2-2\gamma_1)$ does not deviate from $-\frac{1}{2}\pi$ and there is a monotonic transfer of energy from the first to the second harmonic. This is the case studied experimentally by McGoldrick (1970) on a deep water layer. Kim (1970) studied (18) numerically and found, as indicated by the model equation, that initial interactions adjust all relative phase angles to $-\frac{1}{2}\pi$. Simmons (1969) has also discussed solutions of (18) for which γ_i = constant and the relative phase angles are zero but these require particular initial conditions which were not realized in our experiments.

In summary then, the principal influences of non-linear interactions on the change of the relative phase angles are to shorten the cycle of change from that which would be predicted by the linear terms, ΔL_α, and, more important, to adjust initially the relative phase angles to conditions which are favourable for the growth of higher harmonics. After the initial adjustment of the relative phase angles further change is governed by the size of ΔL_α. If ΔL_α is small

enough, the relative phase angle will not change too rapidly from its favourable value and significant growth of the α harmonic is possible.

Since we are considering only quadratic interactions, growth of a higher harmonic is not possible unless all lower harmonics are present. This can readily be seen from (14). Hence, to have a large growth of the α harmonic the linear terms $|\Delta L_\beta|$ on the right side of (18) should be small for all $\beta \leqslant \alpha$. From experiments to be described later, it was deduced that $|\Delta L_\beta|$ should be less than 0·2 when the steepness of the initial sinusoidal wave is in the range $0{\cdot}05 < \epsilon < 0{\cdot}1$.

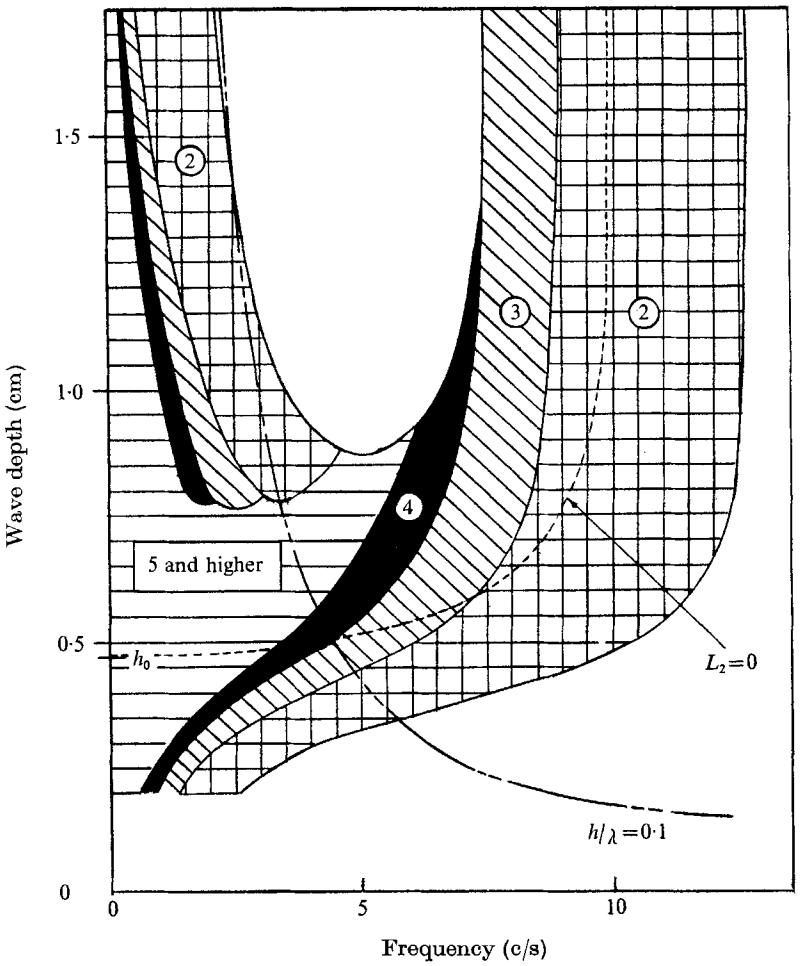

FIGURE 2. Ranges of the growth of higher harmonics.

On the basis of this criterion conditions which are favourable for the growth of a certain harmonic or lower ones have been mapped in figure 2. The numbers in figure 2 indicate the highest harmonic that should be observed in significant amounts. It is not clear that the results on the figure to the left of the curve $h/\lambda = 0{\cdot}1$ are valid since De (1955) has indicated that a Stokes expansion should not be used to describe waves for which $h/\lambda < 0{\cdot}1$.

The curve $L_2 = 0$ in figure 2 shows the decrease of the second-order resonance frequency with the height of the liquid layer. In order to obtain some understanding of the experimental observations on shallow liquid layers, it is of interest to examine the behaviour of L_α for small values of kh:

$$L_\alpha = \tfrac{1}{2}(\alpha^3 - \alpha)\left(\frac{1}{3} - \frac{T}{gh^2}\right)(kh)^2 + O\left\{(kh)^4, \frac{Tk^2}{g}\right\}. \tag{22}$$

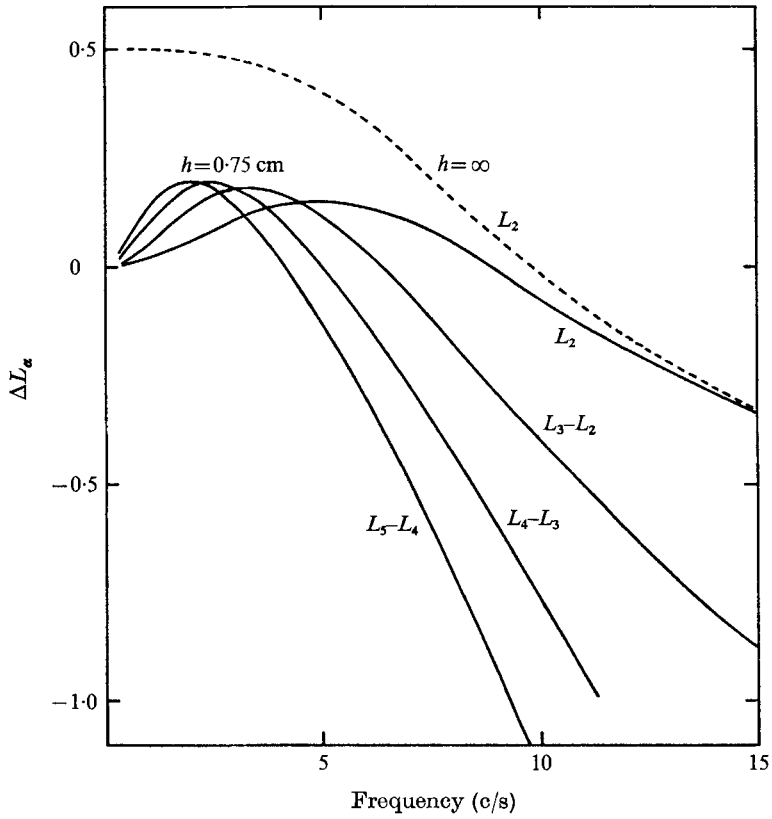

FIGURE 3. Linear terms for water at 25 °C.

As already noted by Phillips (1960), L_α approaches zero for all α as $kh \to 0$ (or $\omega \to 0$). This means that all of the $|\Delta L_\alpha|$ approach zero for small frequencies and that conditions are favourable for the simultaneous growth of a large number of harmonics. It should be noted from (22) that the rate of change of L_α at small kh depends on the depth. At the particular depth $h_0 = (3T/g)^{\frac{1}{2}}$, L_α varies as $(kh)^4$ and one can expect L_α to depart from zero with increasing frequency more slowly than at any other depth. This is reflected in figure 2 by a predicted growth of higher harmonics over a relatively large range of frequencies in the neighbourhood of h_0 (0·48 cm for water). Figure 3 shows plots of $|\Delta L_\alpha|$ for a water depth of 0·75 cm. It can be seen that at this depth the $|\Delta L_\alpha|$ are small enough to be favourable for the growth of the first five harmonics over the frequency range of 0 to 5 c/s.

The simultaneous growth of higher harmonics at shallow depths is further enhanced because the interaction coefficients increase markedly with decreasing depth, as is indicated in figure 4. This arises because at the same wave steepness fluid velocities are larger in shallow layers than in deep layers.

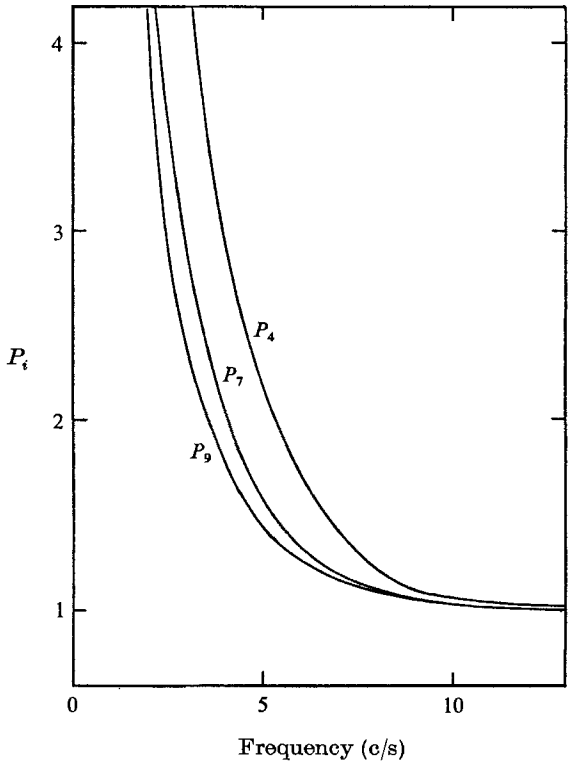

FIGURE 4. Interaction coefficients for $h = 0{\cdot}75$ cm at 25 °C, normalized with respect to the case $h = \infty$.

The interpretation presented in this section neglects the direct formation of a harmonic by interactions of more than two components. It is therefore appropriate to examine the magnitude of this error. The most important triple product term is A_1^3 and its effect will be largest at $L_3 = 0$, where the third harmonic is a free oscillation and A_3 can grow through the quadratic interaction term $A_1 A_2$ in (8) and through the resonant third-order interaction A_1^3. If the A_1^3 term is retained in the analysis, the following simplified equations can be obtained to describe the initial growth of the second and third harmonics from the first harmonic:

$$A_{2,\xi} \simeq -2ikP_4 A_1^2, \tag{23}$$

$$A_{3,\xi} \simeq -\tfrac{4}{3}ikP_7 A_1 A_2 - \tfrac{2}{3}ik^2 P_{13} A_1^3, \tag{24}$$

where

$$P_{13} = (1/8[3K])\{33[K] + 9[3K] - 12[K]^2[2K] - 36[K][2K][3K] + 9k^2T/\omega^2\}.$$

At the initial stage of the interaction A_1 can be approximated by a constant and a simple integration of (23) yields

$$A_3 \simeq kA_1^3(-\tfrac{4}{3}P_7 P_4 \xi^2 - \tfrac{2}{3}iP_{13}\xi). \tag{25}$$

This equation shows that for $\xi > \xi_0 = |P_{13}/2P_4P_7|$ the quadratic interaction dominates the third-order resonant interaction. The values of $t_0 = \xi_0/\omega$ are 0·012 sec for deep-water waves and 0·018 sec for shallow-water waves on a layer of depth 0·75 cm. Thus, almost immediately after the introduction of a sinusoidal wave, quadratic interaction determines the growth of the third harmonic. More conclusive support for the neglect of triple product terms can be obtained when the effects of viscosity are considered since it is found that the ratio of the rate of production of A_3 to direct resonant interaction is small compared to its rate of dissipation by viscosity. This can be shown by adding the term $-\frac{2}{3}ik^2P_{13}A_1^3$ to the right-hand side of the viscous equation (29) below. Numerical integrations of (29) with and without this term reveal negligible differences.

3. Effect of viscosity and the relation between temporal and spatial variations

In order to introduce viscous effects in the analysis, it is assumed that the decay of each Fourier component proceeds independently and that it is given by linear theory. A similar approach has been used by McGoldrick (1965, 1970). The justification for these simplifications is the agreement between predicted and observed wave damping obtained in the experiments.

For a slightly viscous fluid, linear theory predicts

$$dA_\alpha/dt = -\zeta_\alpha A_\alpha, \tag{26}$$

where

$$\zeta_\alpha = \frac{2a^2k^2\nu + (\nu\alpha/8\omega^3)^{\frac{1}{2}}k^2(g+\alpha^2k^2T)\operatorname{sech}^2\alpha kh}{1-(\nu\alpha/2\omega)^{\frac{1}{2}}k\tanh\alpha kh}. \tag{27}$$

This includes viscous effects due to the bottom boundary layer and it reduces to

$$\zeta_\alpha = 2\alpha^2k^2\nu \tag{28}$$

for deep-water waves. Since viscous dissipation is assumed to be independent of the interactions, (8) may be modified as follows:

$$A_{\alpha,\xi} = -(\zeta_\alpha/\omega)A_\alpha + \text{right-hand side of } (\alpha). \tag{29}$$

Due to viscosity the amplitudes undergo damped oscillations and the clear-cut cycles of energy exchange predicted by inviscid theory cannot be observed.

In order to compare (29) with experimental results it is necessary to relate the temporal variations with observed spatial variations. Simmons (1969) showed that for resonant triads the spatial and temporal variations are related through group velocities. This is also true for a system which includes forced oscillations if the group velocity for the αth Fourier harmonic is defined as follows (Kim 1970):

$$C_{g\alpha} = (1/2\omega k)(2k^3\alpha T\tanh\alpha kh + 2\alpha kh\omega^2\operatorname{cosech}2\alpha kh + \omega^2), \tag{30}$$

where $C_{g1} = d\omega/dk$ is the linear group velocity of the first harmonic. When only spatial variations are considered (26) becomes

$$A_{\alpha,x} = -\frac{\zeta_\alpha}{C_{g\alpha}}A_\alpha + \frac{1}{C_{g\alpha}}\text{right-hand side of } (\alpha), \tag{31}$$

and when both spatial and temporal variations are considered,

$$A_{\alpha,\xi}+\frac{C_{g\alpha}}{\omega}A_{\alpha,x}=-\frac{\zeta_\alpha}{\omega}A_\alpha+\text{right-hand side of }(\alpha). \tag{32}$$

Equations (32) are a hyperbolic system of standard form and may be integrated along the characteristic lines to describe transient wave systems if initial conditions are given.

4. Description of experiments

The experiments were performed in a Plexiglas tank 30 ft long, 1 ft wide and 8 in. deep that rests on specially designed spring mounts to isolate it from building vibrations. The water level in the tank was maintained at $3\frac{1}{2}$ in. during experiments. A stainless screen beach was placed at each end of the tank to absorb the incident waves.

It was important to have the interface clean in order to properly account for the dissipation of wave energy. Distilled water was used in all runs. A small amount of sodium chloride (about 0·08 g/l.) was added to increase the electrical conductivity of the liquid. The tank was kept covered to prevent surface contamination and cooling of the interface due to evaporation. Before each experiment the surface of the water was swept clean by a boom that travelled along the entire length of the tank.

Surface elevations were determined by measuring the resistance between two parallel 0·001 in. platinum wires that were supported by a gauge-20 hypodermic needle immersed 1 in. below the water surface. This probe assembly could be moved along as well as across the tank to measure the instantaneous surface elevation at any desired location. A loop circuit, which consists of a 50-ohm resistor in series with the resistance formed between the probe wires when they are immersed in water, was activated by a 5 kHz and 20 V peak-to-peak sinusoidal carrier signal. The signal from the 50-ohm resistor was demodulated to obtain a voltage signal which a static calibration showed to be proportioned to the displacement of the liquid interface. For the shallow-water experiments a platform 4 ft long was placed inside the wave tank and the wave maker was operated at one end of this platform. Wires having diameters 0·003 in. were used in the resistance probe. Although no controlled experiments were performed to check the dynamic response of the probe, it was thought that hysteresis effects were not important. This was justified by the observations that under conditions where interactions were unimportant symmetric sinusoidal wave shapes were recorded by the probe, and that the number of crests detected by the probe agreed with that observed visually.

In the experiments with wave packets a high potential electric wave generator was used. A brass bar of $\frac{1}{4}$ in. diameter was placed across the tank about 5 mm above the water surface. An alternating electric field, with a maximum peak-to-peak voltage of 5 kV, superposed on a 9 kV steady field was applied between the electrode and the water. By modulating the alternating field an amplitude modulated wave packet could be introduced on the water surface. The signal

from the resistance probe was sent to a detector to remove the 5 kHz carrier and the modulation signal was passed to a Honeywell Visicorder (model 906) for display of the wave packet profile as a function of time at a given location from the wave maker.

In steady-state experiments waves were generated by a half immersed Plexiglas dipper of $\frac{3}{16}$ in. thickness that extended over the whole width of the tank and was located in the centre of the tank. This dipper was connected to a cam assembly which was driven by a d.c. motor. By adjusting the eccentricity of the cam assembly the stroke of the wave maker was varied for different operation frequencies to ensure the two-dimensionality of progressive waves. The motion of the wave maker could be monitored by attaching a small magnet on the vertically moving part of the cam assembly. The current from a coil which surrounds the magnet was sinusoidal.

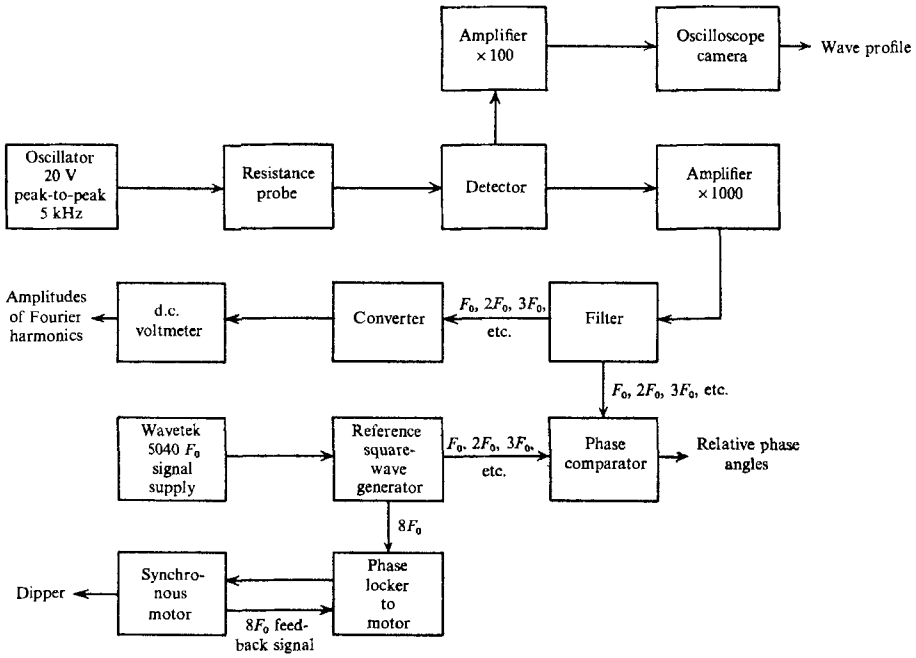

FIGURE 5. Schematic diagram for wave measurements.

A reference signal generator was built to get square signals which have frequencies of F_1 to $10F_1$, where F_1 denotes the frequency of the wave maker. A rotating disk attached to the shaft of the motor had eight evenly spaced slits. A light passed through these slits and activated a photocell which generated a signal with a frequency of $8F_1$. The speed of the motor was controlled by comparing this signal to the $8F_1$ square reference signal.

The demodulated signal from the detector was amplified and displayed on an oscilloscope to take pictures of the wave profile at a particular distance from the wave maker. The signal was also sent to a two-channel filter unit to separate it into different harmonics by tuning the filter to the frequencies of desired harmonics. The separated Fourier harmonics were sent to a phase comparator and

to an a.c./d.c. converter. The d.c. level of the signal was measured with a vacuum-tube voltmeter. In the phase comparator the phases of different harmonics were measured relative to the reference square waves of corresponding frequencies coming from the reference signal generator. The wavelength of the progressive wave could be determined by measuring the distance over which a change of 360° occurred in the phase angle of the first harmonic with respect to a reference square signal to which the motor was phase locked. Figure 5 shows a schematic of the procedure used in our measurements.

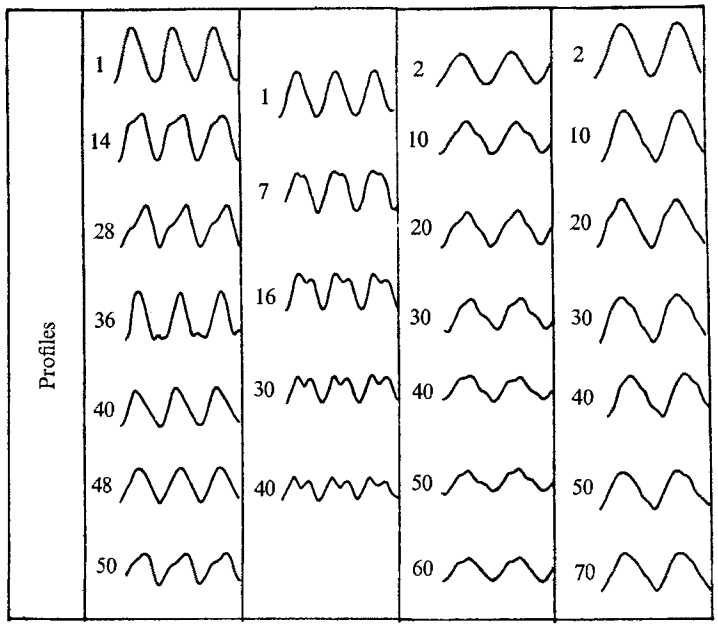

c/s	10·46	9·96	8·40	7·57
n	1·76	1·98	2·99	4·02
°C	25·4	29·1	24·0	26·1
ka_1	0·045	0·061	0·049	0·063

FIGURE 6. Changes of wave profiles on deep water as functions of distance from the wave maker.

5. Results on stationary deep-water waves

When the dipper was operated so that the wave steepness ka_1 was about 0·05 the interface close to the wave maker was sinusoidal. At frequencies in the gravity range or in the capillary range the form of the waves at different distances from the wave maker did not change dramatically. However, over a range of frequencies where both surface tension and gravity are important, 7·5–13 c/s, the type of change depicted in figure 6 was observed.

At frequencies 9·3–13 c/s, except very close to 9·9 c/s, a cyclic growth and decay of the second harmonic occurs. One of these cycles is shown in figure 6 for $n = 1{\cdot}76$ (10·46 c/s). This cyclic change can be explained by equations (18) because for $n = 1{\cdot}76$ the linear term L_2 describing the change of $(\gamma_2 - 2\gamma_1)$ is large

enough to cause a rapid cycle of change but not so large as to nullify energy exchange between the first two harmonics. For $n = 1{\cdot}98$ (9·96 c/s) $L_2 \simeq 0$ and therefore $(\gamma_2 - 2\gamma_1)$ deviates slowly from the favourable phase angle initially set up by non-linear interactions. This facilitates a large and almost monotonic drainage of energy from the first to the second harmonic. The two additional crests evident in the wave profiles for the case of $n = 2{\cdot}99$ (8·4 c/s), $L_3 \simeq 0$, indicate a growth of third harmonic. As discussed in § 2 and indicated in figure 2, this arises because L_2 and $(L_3 - L_2)$ are small enough to ensure a slow change of both $(\gamma_2 - 2\gamma_1)$ and $(\gamma_3 - \gamma_1 - \gamma_2)$. As n increases the wave profile does not change as dramatically. A slight distortion of the wave profile is seen for the case of $n = 4{\cdot}02$ (7·57 c/s). The effects of viscous damping are shown in figure 6 by the decrease in the amplitude of the wave structure with distance from the wave maker.

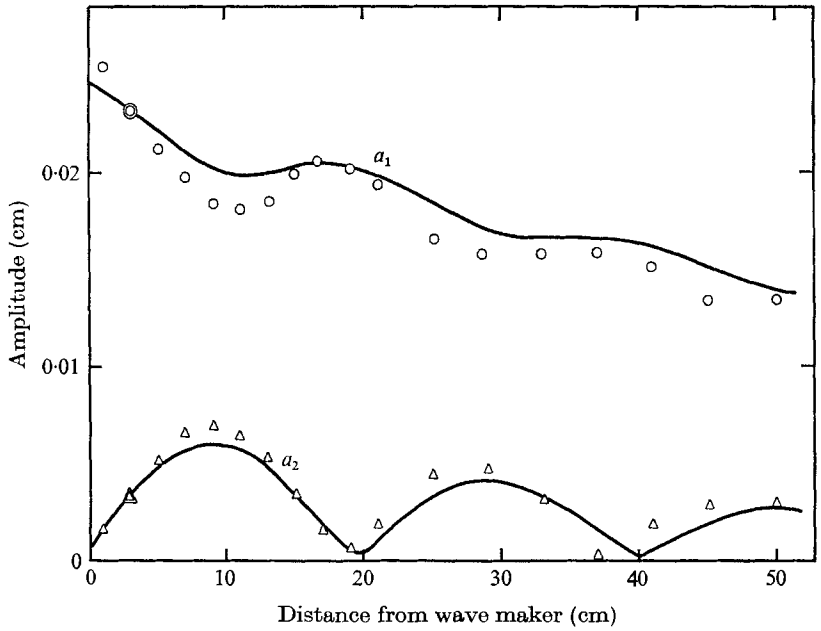

FIGURE 7. Observed variations of Fourier harmonics for $n = 1{\cdot}41$ (11·48 c/s), $\epsilon = ka_1 = 0{\cdot}0793$, temperature = 26·2 °C. ——, predicted; ○, △, measured.

Frequency (c/s)	Depth (cm)	Wavelength (cm)	
		Linear theory	Measured
11·48	Infinite	2·020	2·007
10·44	Infinite	2·247	2·207
9·91	Infinite	2·390	2·393
8·69	Infinite	2·818	2·873
6·97	0·73	3·461	3·452
4·46	0·77	5·809	5·965
3·56	0·754	7·439	7·562
6·16	0·75	4·009	4·014

TABLE 1

Measured values of the amplitudes of the different Fourier harmonics are shown in figures 7, 8 and 9 for $n = 1{\cdot}41$, $n = 1{\cdot}98$ and $n = 2{\cdot}75$. The solid curves were calculated using equations (29) with initial conditions indicated by double circles. Measured values of the relative phase angle $(\gamma_2 - 2\gamma_1)$ are shown in figures 10, 11 and 12 along with curves calculated from equations (5) and (29).

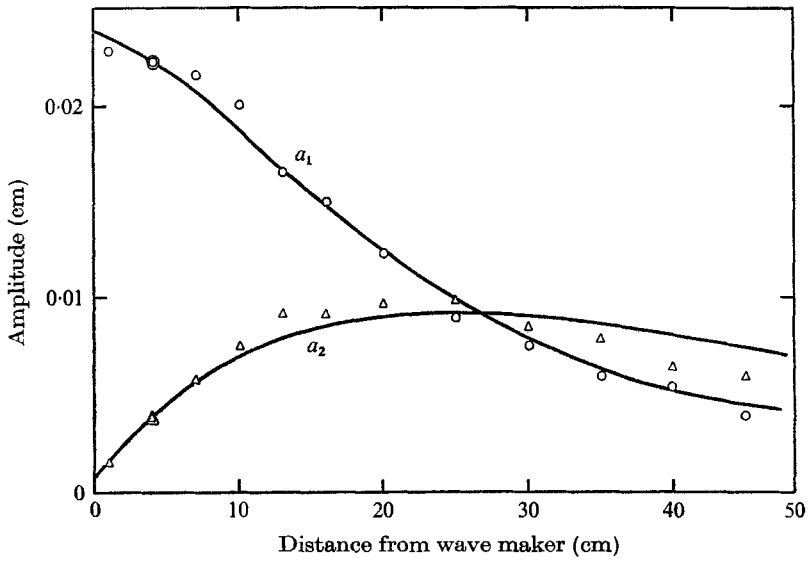

FIGURE 8. Observed variation of Fourier harmonics for $n = 1{\cdot}98$ (9·91 c/s), $\epsilon = ka_1 = 0{\cdot}0605$, temperature = 26·8 °C. ——, predicted; ○, △, measured.

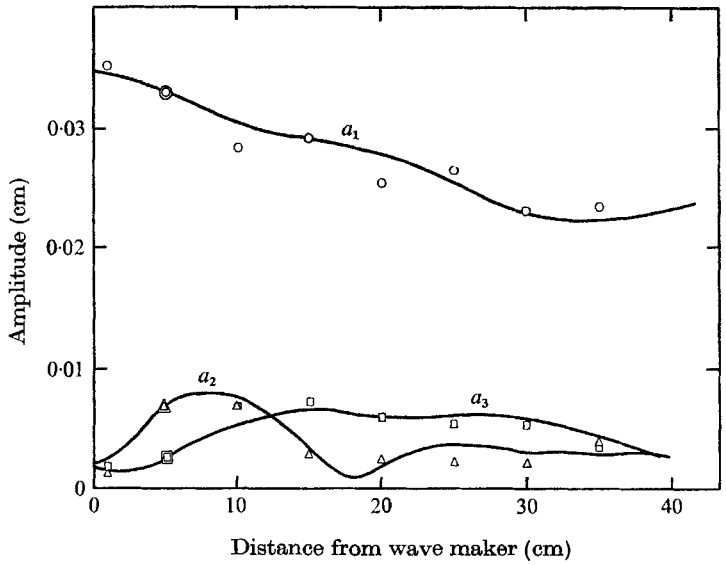

FIGURE 9. Observed variation of Fourier harmonics for $n = 2{\cdot}75$ (8·69 c/s), $\epsilon = ka_1 = 0{\cdot}0761$, temperature = 26·2 °C. ——, predicted; ○, △, □, measured.

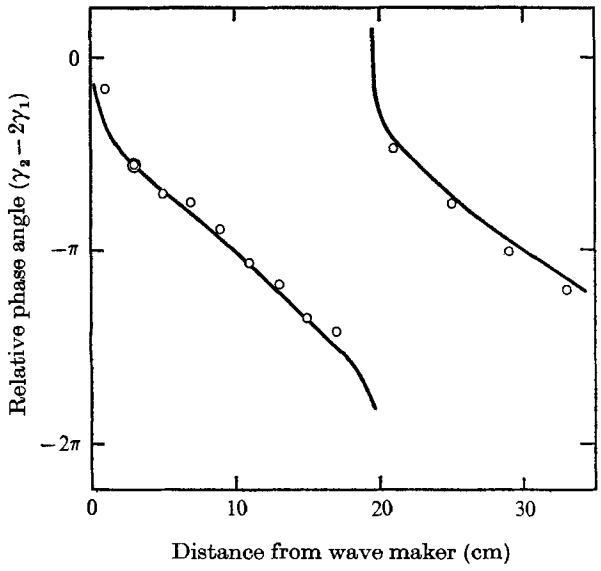

FIGURE 10. Observed variation of the relative phase angle for $n = 1{\cdot}41$.
——, predicted; ○, measured.

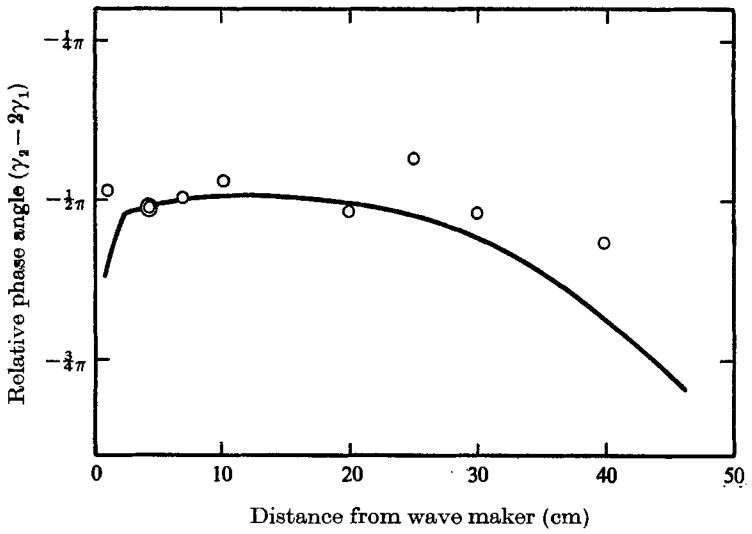

FIGURE 11. Observed variation of the relative phase angle for $n = 1{\cdot}98$.
——, predicted; ○, measured.

Average wavelengths measured over the test section as described in the previous section are given in table 1. These lengths are found to be related to the frequency of the wave maker through the linear dispersion relation (9).

The case of $n = 1{\cdot}98$ corresponds roughly to the resonance condition. In agreement with the discussion in § 2, figure 11 shows that $(\gamma_2 - 2\gamma_1)$ initially adjusts itself to $-\frac{1}{2}\pi$, the condition most favourable for energy transfer between the first and second harmonic. After a_2 has grown to a significant amount the

influence of non-linear interactions on the rate of change of $(\gamma_2 - 2\gamma_1)$ is small. Since $L_2 \simeq 0$ the relative phase angle remains approximately $-\frac{1}{2}\pi$ for the entire range of observation and there is a monotonic drainage of energy from a_1 to a_2. The growth of a_2 is limited because of viscous dissipation. These experimental results supply further confirmation of the theoretical and experimental description of resonant interaction in capillary–gravity waves given by McGoldrick (1965, 1970) and by Simmons (1969).

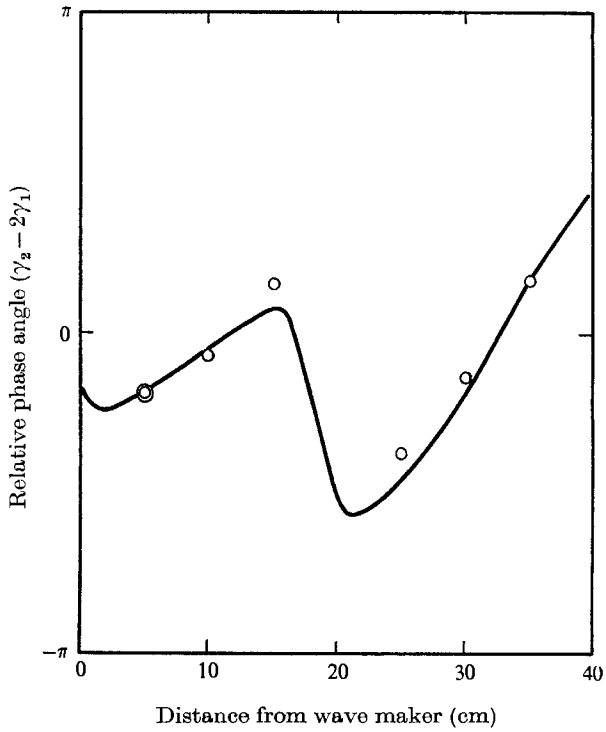

FIGURE 12. Observed variation of the relative phase angle for $n = 2{\cdot}75$. ——, predicted; ○, measured.

The data for $n = 1{\cdot}41$ shown in figures 7 and 10 gives more insight into the interesting phenomenon of cyclic energy exchange. A comparison of figures 7 and 10 indicates that the period governing the cycle of energy exchange between the first and the second harmonic is the same as the period for the change of relative phase angle. A complete cycle of change of $(\gamma_2 - 2\gamma_1)$ for pure capillary waves is calculated to occur in 2·5 wavelengths and, for pure gravity waves, 1 wavelength. As indicated in figure 10, $(\gamma_2 - 2\gamma_1)$ undergoes a complete cycle of change for $n = 1{\cdot}41$ over a distance of about 10 wavelengths. This is in rough agreement with the value of 11 wavelengths calculated from (18) by neglecting non-linear interactions. From figure 10 we see that there is a rather rapid initial change of $(\gamma_2 - 2\gamma_1)$ in the direction of $(\gamma_2 - 2\gamma_1) = -\frac{1}{2}\pi$ due to non-linear interactions. When the amplitude a_2 becomes sufficiently large, or when $(\gamma_2 - 2\gamma_1) \simeq \frac{1}{2}\pi$, the change of $(\gamma_2 - 2\gamma_1)$ is controlled by the linear term L_2 in (18). The amplitude of a_2 increases until $(\gamma_2 - 2\gamma_1)$ reaches a value of $-\pi$ at a distance of about 10 cm.

As indicated by (14), there is a transfer of energy from the second to the first harmonic for $(\gamma_2 - 2\gamma_1)$ between $-\pi$ and -2π. At a distance of about 20 cm a_2 falls to a very small value so that non-linear interactions rapidly adjust $(\gamma_2 - 2\gamma_1)$ to a value of $-\frac{1}{2}\pi$ which is again favourable for the transfer of energy from the first to the second harmonic. The cycle of change is then repeated. It can readily be seen from the above discussion how non-linear interactions tend to shorten the cycle of change over that which would be predicted from linear terms.

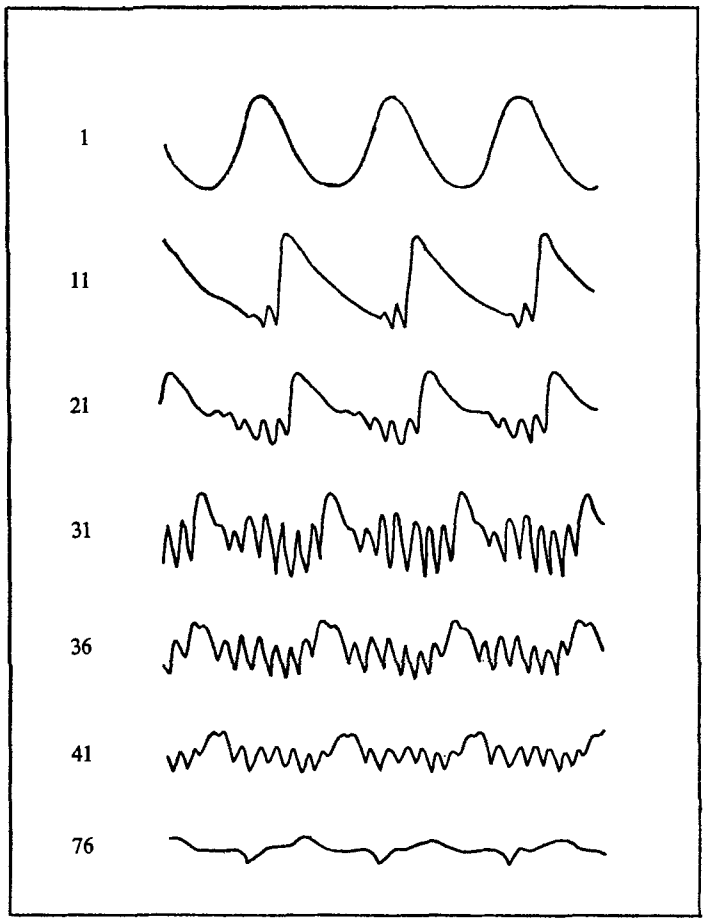

FIGURE 13. Changes in wave profile at 3·036 c/s as functions of distance (cm) from the wave maker. $h = 0{\cdot}65$ cm, $\epsilon = 0{\cdot}0475$, temperature = 22 °C.

The growth of the third harmonic at $n = 2{\cdot}75$ is depicted in figure 9. The third harmonic appears only after an appreciable growth of the second harmonic. The relative phase angle $(\gamma_2 - 2\gamma_1)$ increases initially because L_2 is a positive number at $n = 2{\cdot}75$. The amplitude of the second harmonic a_2 at first increases but then decreases because of energy transfer to the third harmonic; a_2 falls to a very small value, at a distance of about 18 cm, before $(\gamma_2 - 2\gamma_1)$ can increase to π. Non-linear interactions then cause a rapid readjustment to an angle which is favourable for the transfer of energy from a_1 to a_2.

6. Results with shallow water layers

If the wave maker is operated at 9·86 c/s and the height of the liquid layer is decreased the monotonic growth of second harmonic observed on deep layers (see figure 6 for $n = 1{\cdot}98$) changes to a cyclic growth and decay of the type shown in figure 6 for $n = 1{\cdot}76$. As predicted by theory (see the locus of $L_2 = 0$ in figure 2), the observed frequency for resonant growth of the second harmonic decreased with decreasing depth. For example, at $h = 0{\cdot}714$ cm resonance was observed at 8·79 c/s (24·5 °C) and at 0·635 cm it was at 8·12 c/s (23·6 °C).

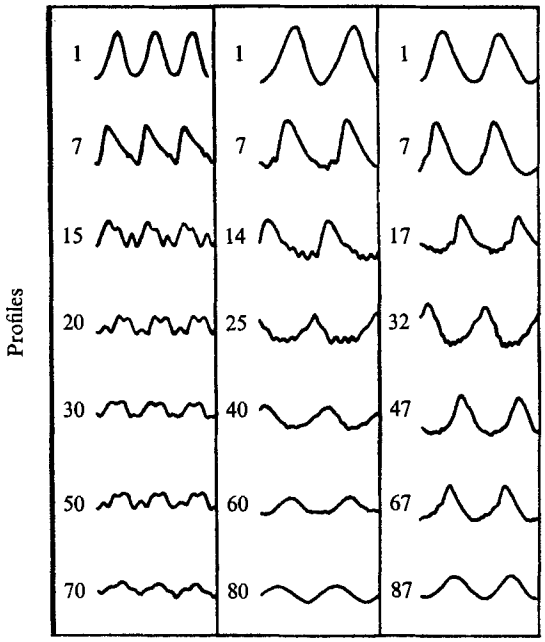

h	0·730	0·730	0·770
c/s	6·973	4·453	4·005
°C	23·8	20·6	25·0
ka_1	0·0840	0·0700	0·0591

FIGURE 14. Change of wave profile near a depth of 0·75 cm as a function of distance from the wave maker.

A more spectacular growth of higher harmonics could be observed in shallow layers than in deep layers. Figure 13 shows observed changes of the wave profile on a layer of 0·65 cm with the wave maker operating at 3·04 c/s. The appearance of seven additional crests indicate a large growth of the eighth harmonic. The initial steepening of the primary wave is due mainly to growth of the second harmonic. Values of ΔL_α for this condition are shown in table 2. It should be noted that all of them are less than 0·2 with the exception of $L_9 - L_8$.

Observed wave profiles on a water layer of 0·75 cm are shown in figure 14. At high enough frequencies the sinusoidal wave pattern does not change its shape as it propagates. As suggested by figure 2, successively higher harmonics appeared

as the frequency decreased. Figure 15 shows the change of wave pattern observed as the height of the water layer is decreased with the wave maker operating at 5·12 c/s. Again the observations are qualitatively in agreement with the predictions in figure 2. On deep water layers the sinusoidal wave pattern does not change. At a depth of 0·79 cm four additional crests can be observed. At 0·55 cm we see two additional crests, indicating appreciable growth of the third harmonic. At 0·47 cm these two additional peaks are not as large as at 0·55 cm. Values of ΔL_α associated with the shallow-water experiments are shown in table 2.

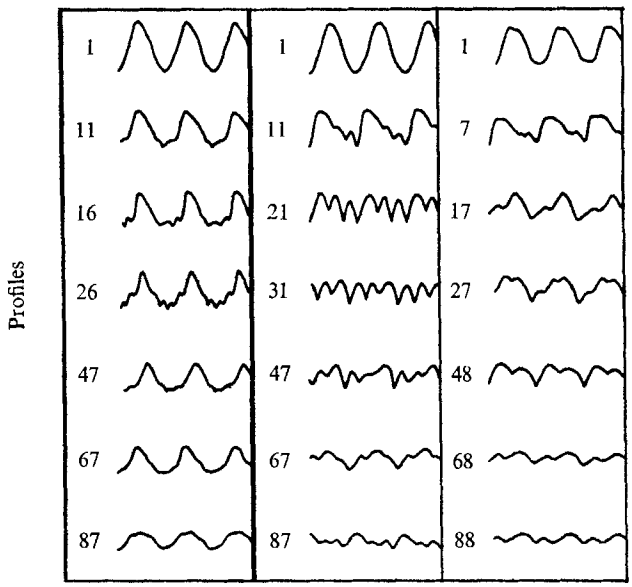

h	0·79	0·55	0·47
c/s	5·115	5·118	5·155
°C	23·5	23·7	23·9
ka_1	0·0764	0·0565	0·0671

FIGURE 15. Change of wave profile near a frequency of 5 c/s as a function of distance from the wave maker.

The interaction equations developed in §§ 2 and 3 are valid only if the highest harmonic present is the fourth. It seems therefore they cannot be applied to all of the experimental observations made with shallow water layers. However, good agreement was obtained with experimental measurements for cases in which they are applicable. Figures 16 and 17 compare calculated and measured amplitudes and phase angles for a 0·75 in. layer when the wave maker is operated at 6·11 c/s.

7. Results on viscous damping

The wave-energy ratio is given as

$$\frac{E}{E_0} = \frac{\Sigma_\alpha \alpha C_{g\alpha} a_\alpha^2 I_\alpha}{\Sigma_\alpha \alpha C_{g\alpha} a_{\alpha 0}^2 I_\alpha}, \tag{33}$$

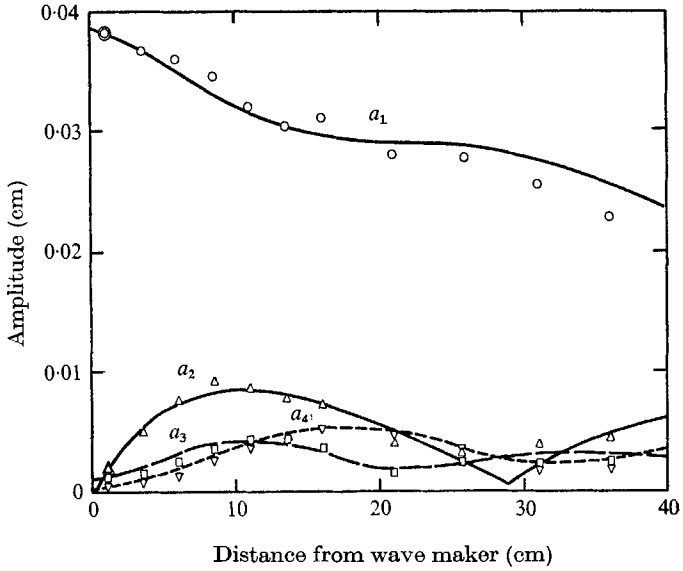

FIGURE 16. Observed variation of Fourier harmonics for $h = 0{\cdot}75$ cm ($L_4 \simeq 0$), 6·16 c/s, temperature = 22·7 °C. ——, – –, - - -, predicted; ○, △, □, ▽, observed.

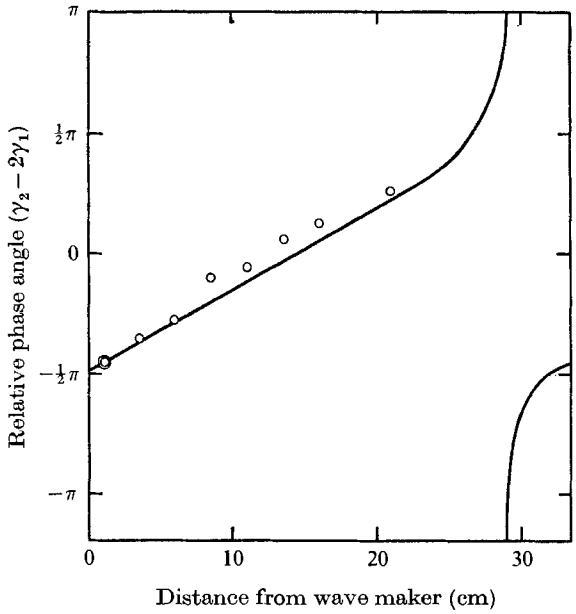

FIGURE 17. Observed variation of the relative phase angle for $h = 0{\cdot}75$ cm ($L_4 \simeq 0$). ——, predicted; ○, measured.

Depth (cm)	Frequency (c/s)	L_2	L_3-L_2	L_4-L_3	L_5-L_4	L_6-L_5	L_7-L_6	L_8-L_7	L_9-L_8
0·73	6·97	0·096	−0·070	−0·288	−0·512	−0·737	−0·962	−1·187	−1·412
0·77	4·46	0·155	0·163	0·082	−0·025	−0·139	−0·255	−0·370	−0·486
0·754	3·56	0·127	0·184	0·156	0·089	−0·009	−0·077	−0·165	−0·253
0·650	3·04	0·072	0·120	0·109	0·058	−0·014	−0·096	−0·183	−0·272
0·79	5·12	0·167	0·132	0·017	−0·115	−0·251	−0·387	−0·524	−0·660
0·55	5·12	0·028	−0·054	−0·209	−0·392	−0·585	−0·780	−0·977	−1·173
0·47	5·12	−0·041	−0·165	−0·348	−0·561	−0·786	−1·016	−1·248	−1·481

TABLE 2

where the subscript 0 represents some reference point in space. Calculated values of this ratio for a frequency of 9·91 c/s are compared in figure 18. The straight line represents wave-energy dissipation which one would expect if the wave profile kept its initial sinusoidal form. The good agreement between theory and experiment indicates that the interface was clean and that viscous dissipation was properly accounted for in the experiments. The marked increase in viscous dissipation because of the generation of higher harmonics is clearly demonstrated.

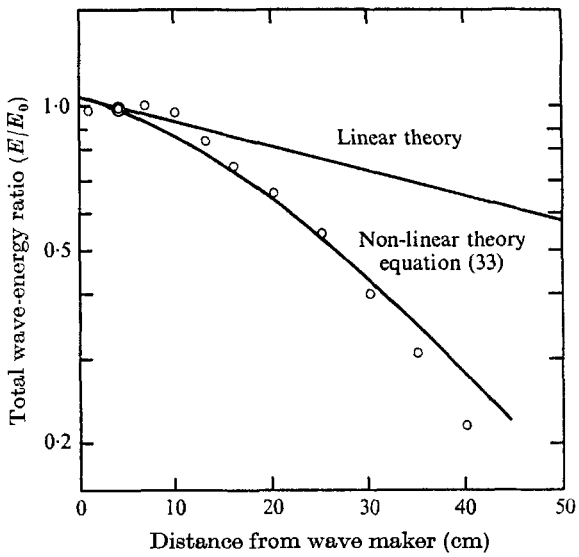

FIGURE 18. Observed dissipation of wave energy for $n = 1{\cdot}98$. ○, measured.

8. Results on wave packets

Wave packets with approximately 10 waves in one envelope and with a maximum steepness of $ka_1 \sim 0{\cdot}03$ were studied. Distortion was observed for $n = 1{\cdot}48$ to 2·95, but the most spectacular results were obtained close to the resonance condition. Figure 19 shows the change of the wave packet as it propagates for the case $n = 2{\cdot}01$. It is seen that the second harmonic formed by non-linear interactions eventually accumulates in the front part of the packet because it has a higher group velocity than the first harmonic. The group velocity of the first harmonic has been calculated from the distance between the probe and the wave maker and the time elapsed between the input of an electric signal to the wave maker and the detection of a signal by the probe. Observed group velocities are in good agreement with those predicted by linear theory.

This work has been supported by the National Science Foundation under grant NSF GK 3792 and NSF GK 13748. Much of the electronic equipment used in this study was designed by Mr R. Anderson in the Electronic Shop of the Department of Chemical Engineering, University of Illinois.

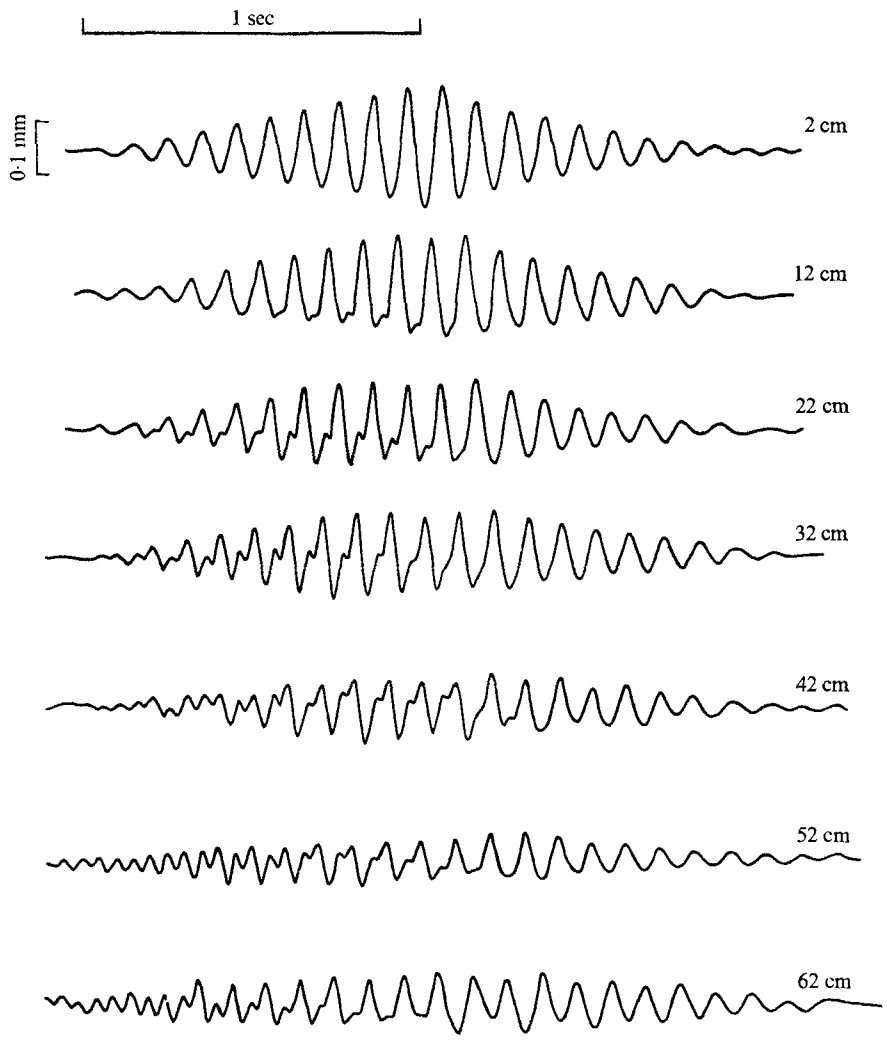

FIGURE 19. Development of a wave packet at $n = 2{\cdot}021$ (9·81 c/s) with distance from wave maker.

REFERENCES

BENJAMIN, T. B. & FEIR, J. E. 1967 *J. Fluid Mech.* **27**, 417–430.

BENNEY, D. J. 1962 *J. Fluid Mech.* **14**, 577–584.

BRETHERTON, F. P. 1964 *J. Fluid Mech.* **20**, 457–479.

DE, S. C. 1955 *Proc. Camb. Phil. Soc.* **51**, 713–736.

KIM, Y. Y. 1970 Ph.D. thesis in Chemical Engineering, University of Illinois.

LONGUET-HIGGINS, M. S. & SMITH, N. D. 1966 *J. Fluid Mech.* **25**, 417–436.

MCGOLDRICK, L. F. 1965 *J. Fluid Mech.* **21**, 305–331.

MCGOLDRICK, L. F. 1970 *J. Fluid Mech.* **40**, 251–271.

MCGOLDRICK, L. F., PHILLIPS, O. M., HUANG, N. E. & HODGSON, T. H. 1966 *J. Fluid Mech.* **25**, 437–456.

PHILLIPS, O. M. 1960 *J. Fluid Mech.* **9**, 193–217.

PIERSON, W. J. & FIFE, P. J. 1961 *Geophys. Res.* **66**, 163–179.

SIMMONS, W. F. 1969 *Proc. Roy. Soc.* A **309**, 551–575.

WILTON, J. R. 1915 *Phil. Mag.* **29**, 688–600.